RSC Advances

PAPER

View Article Online
View Journal | View Issue

Cite this: *RSC Adv.*, 2021, **11**, 24526

Optical studies and dielectric response of $[DMA]_2MCl_4$ (M = Zn and Co) and $[DMA]_2ZnBr_4$

N. Mahfoudh, K. Karoui and A. BenRhaiem *

$[DMA]_2ZnCl_4$, $[DMA]_2CoCl_4$ and $[DMA]_2ZnBr_4$ crystallized in the monoclinic system, in the $P2_1/n$, $P2_1/n$ and $P2_1/c$ space groups, respectively. The optical properties of $[DMA]_2MCl_4$ (M = Zn and Co) and $[DMA]_2ZnBr_4$ were studied using ultraviolet-visible (UV-Vis) spectroscopy in the range of 200–800 nm. The Tauc model was used to determine the band gap energy of each hybrid compound. The calculated values of the direct and indirect band gaps (E_{gd}, E_{gi}) for all samples were found to be in the range of 1.91 eV to 4.29 eV for $[DMA]_2ZnCl_4$, 4.76 eV to 5.34 eV for $[DMA]_2ZnBr_4$ and 1.77 eV to 3.84 eV for $[DMA]_2CoCl_4$. The Urbach energy (E_u), extinction coefficient (k) and refractive index (n) of each compound was calculated. On the other hand, the dispersion of (n) is discussed in terms of the single oscillator Wemple–DiDomenico model. The single oscillator energy (E_0), the dispersion energy (E_d), and both the real ε_r and imaginary parts ε_i of the dielectric permittivity were estimated. The variation of optical conductivity with the incident photon energy has also been studied. We employed impedance spectroscopy to thoroughly investigate the dipolar dynamics in the prepared materials. The evolution of the dielectric loss, as a function of frequency, showed a distribution of relaxation times, which probably could be of a Maxwell–Wagner type interfacial polarization relaxation, possibly attributed to grain boundary effects or blocking at the contacts. In fact, the current work opens an efficient path to high quality organic–inorganic halide perovskites with good optical properties, which makes them suitable for application in nonlinear optoelectronic devices.

Received 10th May 2021
Accepted 6th July 2021

DOI: 10.1039/d1ra03652a

rsc.li/rsc-advances

1. Introduction

$[N(CH_3)_2H_2]_2ZnCl_4$, $[N(CH_3)_2H_2]_2CoCl_4$ and $[N(CH_3)_2H_2]_2ZnBr_4$ (here in after $[DMA]_2MeX_4$ (Me = Zn and Co and X = Cl and Br)) are members of the A_2MeX_4 crystal family, which have been extensively studied as typical materials showing various successive phase transitions when the temperature varies. On the other hand, the A_2MeX_4 type crystals are interesting because of their many physical properties related to the ferroelectric and commensurate or incommensurate phase transitions. Moreover, most of these materials show many physical properties related to structural phase transitions at low temperatures. Therefore, these fundamental properties make the crystal family suitable for several applications, such as temperature and humidity sensors, and memory effects that manifest themselves as temperature anomalies in their physical properties.[1–3]

Dimethylammonium tetrachlorozincate $[DMA]_2ZnCl_4$, dimethylammonium tetrachlorocolbatate $[DMA]_2CoCl_4$ and dimethylammonium tetrabromozincate $[DMA]_2ZnBr_4$ crystals have turned out to be very interesting members belonging to an A_2MeX_4 that undergoes different phase transitions at and below room temperature. In fact, at room temperature, $[DMA]_2ZnCl_4$ crystallizes in the monoclinic system with the $P2_1/n$ space group. Then, the refined parameters are: a = 13,297 Å, b = 8,620 Å, c = 11 494 Å and β = 89, 8°.[4,5] However, the phase transition temperatures of $[DMA]_2ZnCl_4$ have not yet been correctly established. Therefore, an investigation of optical birefringence and piezoelectric coefficients revealed a range of phase transitions occurring at 217 K, 238 K, 250 K, 272 K, 295 K, and 310 K.[6] Therefore, the temperatures of some phase transitions were determined through investigations of specific heat at 151 K, 240 K, 253.9 K, 272.2 K, 298.3 K, and 309.1 K.[7] In addition, heat capacity measurements showed phase transitions at 201 K, 250 K, 272 K, and 310 K.[8] Moreover, the occurrence of phase transitions at 444 K was confirmed by DSC measurements.[9] Monoclinic crystals of $[DMA]_2CoCl_4$ are of the space group $P2_1/n$. Unit cell dimensions are as follows: a 8.5313 Å, b = 11.4382 Å, c = 13.3070 Å and β = 90.038°.[10] The transition temperatures of $[DMA]_2CoCl_4$ are T_1 = 292 K, T_2 = 319 K, T_3 = 365 K, T_4 = 374 K and T_5 = 444.[11] At 291 K, $[DMA]_2ZnBr_4$ crystallizes in the monoclinic system with the $P2_1/c$ space group and its unit cell parameters are a = 8.706 (6) Å, b = 11.956 (64) Å, c = 16.289 (95) Å, β = 121.84°, and Z = 4. The $[DMA]_2ZnBr_4$ crystal undergoes four phase transitions at T_1 = 281 K, T_2 = 340 K, T_3 = 377 K, and T_4 = 408 K.[12]

Theoretical and experimental studies of different crystals with dialkylammonium cation showed that the change of the hydrogen bond network considerably influences the lattice

Laboratory of Spectroscopic Characterization and Optic Materials, Faculty of Sciences, University of Sfax, B. P. 1171, 3000 Sfax, Tunisia. E-mail: abdallahrhaiem@yahoo.fr

dynamics and manifests itself in an essential transformation of the crystalline structure. Therefore, due to the availability of H bonds, the above compounds are expected to be proton conductors. As a consequence, they are important because of the proton transport mechanisms in biophysical processes and their employment in numerous electrochemical devices, such as batteries, fuel cells, chemical sensors, electrochromic devices, and super capacitors.[13]

During the past years, optical studies have been performed on organic–inorganic nanocomposites. These studies have evolved towards different objectives, such as the development of materials with specific optical properties based on the properties of organic and inorganic chromophores. In fact, because of their several advantages for designing materials for optical applications (versatile and relatively facile chemistry, materials having good mechanical integrity and excellent optical quality), numerous hybrid organic–inorganic materials have been developed in the past few years. The chemical industry has tended to frequently use organometallic complexes because they use a minimum of energy by participating in chemical reactions in the transformation of natural elements. It should also be noted that organometallic complexes are known for their interesting luminescence properties, which have recently played an important role, particularly as phosphorescent components for light-emitting diodes OLEDs "Organic Light-Emitting Diodes".[14] In fact, the most striking examples of functional hybrids exhibit emission properties (solid-state dye laser, rare-earth doped materials), absorption properties (photochromic), and non linear optical (NLO) properties.[15–17] The growth of research in nonlinear optics (NLO) is mainly related to the rapid technological advancements that have occurred in several related fields, such as ultra-fast phenomena, optical communication and optical storage devices. On the other hand, nonlinear optical crystals, which have high optical band gap, ultrafast response times and low dielectric constant, are in great demand in the optical storage devices, color display units and optical communication systems, *etc.*18 Moreover, compared to organic molecules, organometallic compounds showed strong absorptions in UV/V regions due to metal-to-ligand and ligand-to-metal charge transfer.[19] On the other hand, all the properties combine to make them as a suitable candidate for multifunctional material development.[20] In fact, several studies were performed on $[TMA]_2MeX_4$ compounds due to their variety of phase transitions. The obtained results indicate that the tetramethylammonium and the tetrachlorozincate $[TMA]_2ZnCl_4$ crystal is suitable for optoelectronic applications around room temperature. Below 296 K, this crystal can directly store the optical data and information. Moreover, the $[TMA]_2ZnCl_4$ crystal is conveniently transparent in the visible light region with low absorption coefficient in this region, which makes it suitable for anti-reflection layers of solar.[21] However, the previous optical studies on the use of organic–inorganic hybrid materials in optoelectronic or optical application have received little attention. In fact, to use materials in the field of optoelectronics, it is necessary to know their optical constants. Additionally, optical measurements can give us a lot of information about the composition and the quality of the materials.

In fact, in the present paper, we have investigated the optical properties of $[DMA]_2MCl_4$ (M = Zn, Co) and $[DMA]_2ZnBr_4$ compounds. The results of the optical absorption were performed at room temperature. The main aim is to determine some important optical parameters, such as the bandgap energy (E_g), the Urbach energy (E_u), the refractive index (n), the oscillator energy (E_0), the dispersion energy (E_d), the real and imaginary parts of the complex dielectric function (ε) and the optical conductivity σ_{opt}. We have also made an analysis of optical properties correlated with dielectric properties of $[DMA]_2MCl_4$ (M = Zn, Co) and $[DMA]_2ZnBr_4$ single crystals. These results were analyzed and discussed in the light of published data of some A_2MX_4 crystals.

2. Experiment

$[DMA]_2MCl_4$ (M = Zn, Co) crystals are prepared by dissolving stoichiometric amounts of water *starting materials* $N(CH_3)_2H_2Cl$ and MCl_2 (M = Zn, Co) in water, in a molar ratio of (2 : 1) according to the reaction scheme:

$$2[N(CH_3)_2H_2]Cl + MCl_2 \rightarrow [N(CH_3)_2H_2]_2MCl_4$$

After a few days of evaporation, deep blue single crystals of $[DMA]_2CoCl_4$ and white polyhedral crystals $[DMA]_2ZnCl_4$ appeared then stored in a sealed container in order to carry out the planned studies. The crystals grew as elongated prisms.

As in the case of the compound, the $[DMA]_2ZnBr_4$, $ZnBr_2$ anhydrous (Sigma-Aldrich) (1 mmol) and $(CH_3)_2NH{\cdot}HCl$ (Sigma-Aldrich) (2 mmol) were dissolved in a hydrobromic acid aqueous solution (30 mL) and stirred after which the obtained solution had slowly been evaporated at RT for a few days. Then, the white prism-like single crystals of $[DMA]_2$ $ZnBr_4$ were collected, washed with a small amount of distilled water, and dried in open air.

3. Apparatus

The X-ray diffraction (XRD) pattern of powder was recorded at room temperature using a Philips PW 1710 diffractometer operating with copper radiation ($\lambda K_\alpha = 1.5406$ Å) in a range of Bragg's angle ($5° \leq 2\theta \leq 80°$) in each compound. Then, the unit cell parameters were refined with the Celref 3 software[22] by the least square method from the powder data.

Therefore, in order to study the optical properties of $[DMA]_2MCl_4$ (M = Zn, Co) and $[DMA]_2ZnBr_4$ compounds, the UV-Vis spectra were obtained by a UV-VIS spectrophotometer (Shimadzu UV-3101PC) using a source emitting wavelength radiations varying between 200 and 800 nm on a pellet of each compound. For the optical measurements, we used crystal powder pellets of 8 mm diameter and 0.8 mm thick.

The dielectric measurements were carried out on a pellet of 8 mm diameter and 1.1 mm thick obtained by means of a press of 3 tons per cm^2 from a finely ground powder, using a SOLARTRON SI 1260 impedance bridge, which operates in the frequency range of 10^{-1} to 10^7 Hz. Then, the temperature is

regulated using a precise regulator fitted with a thermocouple placed near the sample.

4. Results and discussion

4.1. X-ray diffraction study

The powder X-ray diffraction pattern of $[DMA]_2MCl_4$ (M = Zn, Co) and $[DMA]_2ZnBr_4$, recorded at room temperature is shown in Fig. 1. In fact, all the peaks of $[DMA]_2ZnCl_4$ are indexed in the monoclinic system with the $P2_1/n$ space group while the unit cell parameters refined by the least square method are: $a = 13.201$ Å, $b = 8.604$ Å, $c = 11.552$ Å and $\beta = 89.34°$. These values are in good agreement with those found in the literature.[4,5]

The $[DMA]_2CoCl_4$ compound at 300 K belongs to a mono-clinic system, $P2_1/n$ space group, with the following unit cell dimensions: $a = 8.5393$ Å, $b = 11.3905$ Å, $c = 13.4069$ Å and $\beta = 91.02°$. Then, compared to the standard value, the obtained diffraction peak positions are found to be in agreement with those of the corresponding literature, confirming the phase and purity of the compound.[10]

Moreover, all the reflection peaks corresponding to 2θ values of $[DMA]_2ZnBr_4$ are indexed monoclinic system with the $P2_1/n$ space group. The obtained lattice parameters are $a = 8.7163$ Å, $b = 11.9837$ Å, $c = 16.1951$ and $\beta = 121.59°$. These results are in agreement with the published results.[12]

4.2. Optical absorption

Fig. 2(a) shows electronic absorption spectra of $[DMA]_2ZnCl_4$, in comparison to $[DMA]_2ZnBr_4$. In fact, in the UV region, a broad absorption band corresponds to three peaks for each compound. The absorption increases sharply at 222 nm and 213 nm, which is the characteristic of the fundamental band of $[DMA]_2ZnCl_4$ and $[DMA]_2ZnBr_4$ materials, respectively. It is due to the excitation of an electron from the valence band to the conduction band, *i.e.* band-to-band transition, in the $[ZnCl_4]^{2-}$ and $[ZnBr_4]^{2-}$ tetrahedron, indicating the material gap. However, the other two bands observed at (283 nm, 370 nm) for $[DMA]_2ZnCl_4$ and at (256 nm, 371 nm) and for $[DMA]_2ZnCl_4$, are

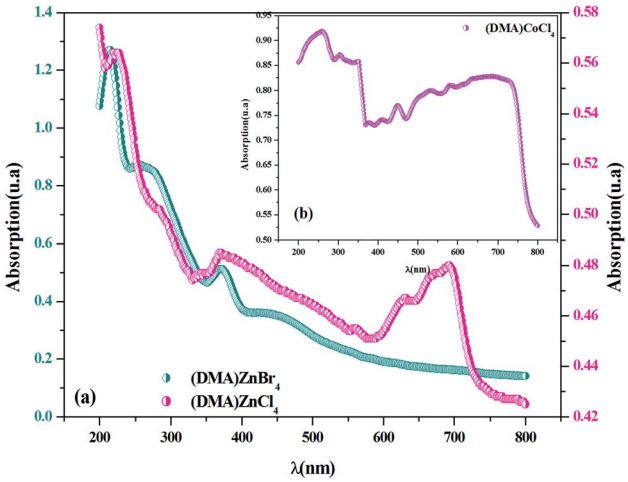

Fig. 2 (a and b) UV-visible absorption spectra for $[DMA]_2ZnCl_4$, $[DMA]_2ZnBr_4$and $[DMA]_2CoCl_4$ at room temperature.

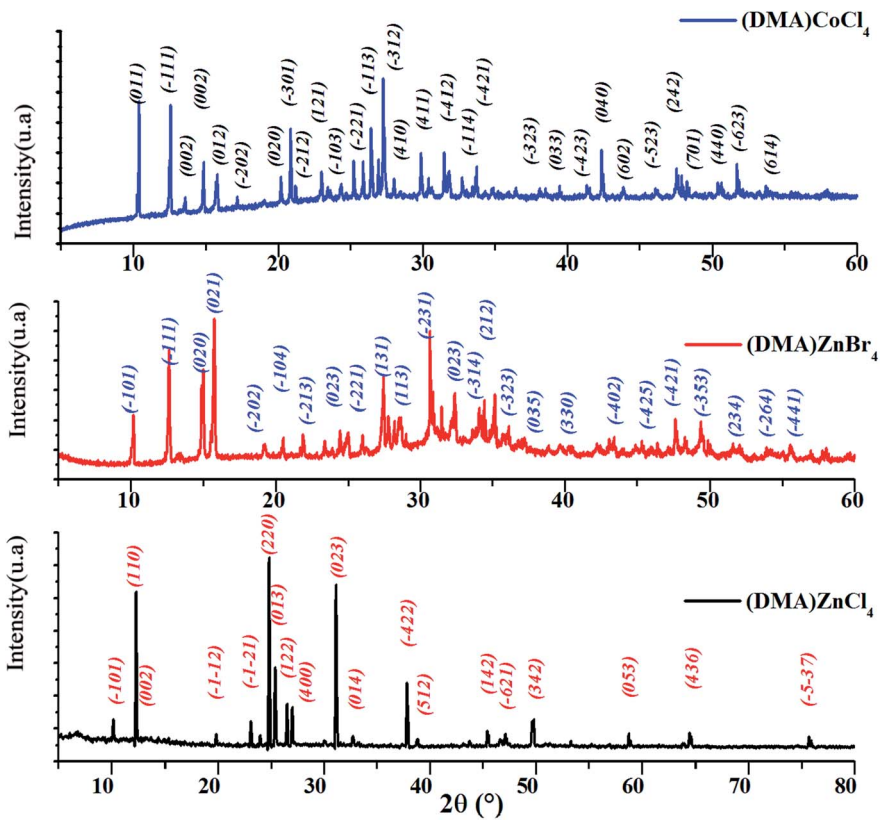

Fig. 1 X-ray diffraction pattern of $[DMA]_2ZnCl_4$, $[DMA]_2CoCl_4$ and $[DMA]_2ZnBr_4$.

Table 1 Assignment of absorption bands in spectrum of $[DMA]_2CoCl_4$

Band (nm)	Transition from $^4A_2(^4F)$
258	$^2T_1(^2F)$
304	$^2A_2$, $^2T_2(^2F)$
376	$^2E(^2D)$
405	$^2T_2(^2D)$
448	$^2T_1$, $^2T_2$, ^2E, $^2T_1$, $^2T_1(^2P^2H)$
534	$^2T_1$, $^2A_1$, $^2T_2(^2G)$
579	$^4T_1(^4P)$
635	$^2E(^2G)$

attributed to the excitonic transition. These results are quite similar to those found for other previously reported MX^{4-} hybrids, such as $[(C_2H_5)NH_3]_2ZnCl_4$ and $[N(CH_3)_4]_2ZnCl_4$.[23,24] As for its structure, $[DMA]_2ZnCl_4$ is close to isomorphous tetramethylammonium. The observed band positions are very similar to the $[TMA]_2ZnCl_4$ spectrum.[25] The peak around 692 nm in $[DMA]_2ZnCl_4$ spectrum can be assigned to –NH– species.

Fig. 2(b) shows the experimental UV-Vis absorption spectrum of $[DMA]_2CoCl_4$ at room temperature. As previously seen, there are eight distinct absorption peaks. The spectrum shows three absorption bands in the UV region centered at 376 nm, 304 nm and 258 nm, corresponding to the low energy tail of the band, corresponding to ligand-to-metal charge transfer (3p Cl ! 3d Co).[26] Additionally, the absorption spectrum exhibits five peaks in the visible domain, located at 635 nm, 579 nm, 534 nm, 448 nm and 405 nm, probably assigned to internal electron transitions of the 3 d^7 configuration of a Co^{2+} ion in $[CoCl_4]^{2-}$.[27–29] The observed band positions are very similar to those found in other materials containing organic–inorganic hybrid compound previously reported in the literature.[26,30–32] As expected from some literature data, the corresponding transitions from the initial $^4A_2(^4F)$ state into the excited states are grouped in Table 1.[30,32] It is also interesting to note that with respect to the mutual position of the bands, the $[DMA]_2CoCl_4$ spectrum is very close to the $[TMA]CoCl_4$ spectrum.[27] In the UV region, one can observe that the absorbance values of the Br-based compound are higher than those of the Cl-based compounds. Moreover, from absorption spectra, the crystals absorb UV radiation, which may be used as an effective UV shelter.[33]

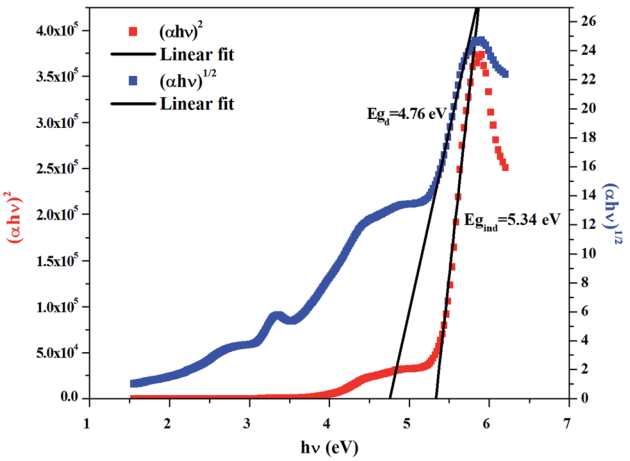

Fig. 4 Variations of $(\alpha h\nu)^2$ and $(\alpha h\nu)^{1/2}$ as a function of the photon energy for the compound $[DMA]_2ZnBr_4$.

4.3. Direct and indirect optical band gap and Urbach energy

The band gap energy is determined using the Tauc relation:[34]

$$\alpha h\nu = B(h\nu - E_g)^n \quad (1)$$

with α the optical absorbance, $h\nu$ the photon energy, B a constant, then E_g the optical band gap, $n = \frac{1}{2}$ or 2 for direct and indirect allowed transition, respectively.

The dependence of $(\alpha h\nu)^2$ and $(\alpha h\nu)^{1/2}$ on the photon energy is shown in Fig. 3–5 for $DMA]_2ZnCl_4$, $[DMA]_2ZnBr_4$ and $[DMA]_2CoCl_4$compounds, respectively. Then, the obtained intersection of the straight line, which is divided by the slope, is equal to the energy band gap of optical transitions.[35] On the other hand, the optical edge or gap was inferred by linear

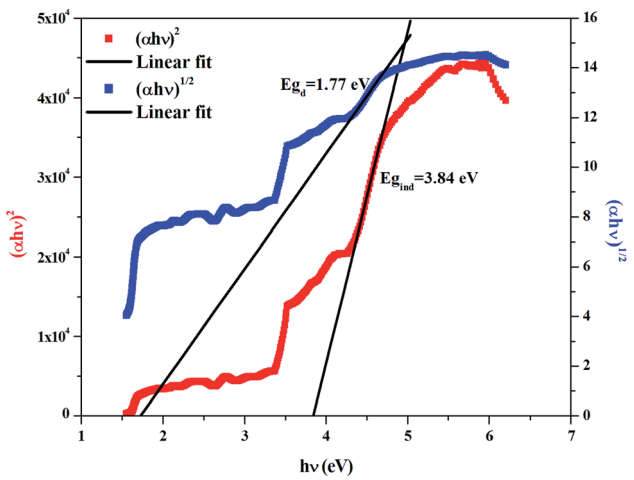

Fig. 3 Variations of $(\alpha h\nu)^2$ and $(\alpha h\nu)^{1/2}$ as a function of the photon energy for the compound $[DMA]_2ZnCl_4$.

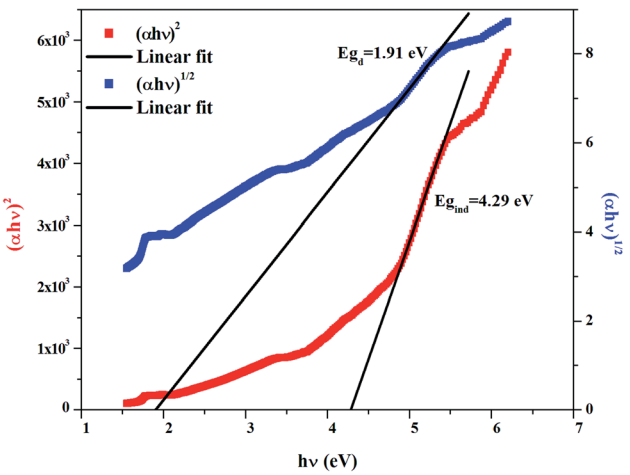

Fig. 5 Variations of $(\alpha h\nu)^2$ and $(\alpha h\nu)^{1/2}$ as a function of the photon energy for the compound $[DMA]_2CoCl_4$.

Table 2 Calculated values of band gaps and Urbach energy

Sample	E_{gd} (eV)	E_{gi} (eV)	E_u (eV)
$[DMA]_2ZnCl_4$	1.91	4.29	2.19
$[DMA]_2ZnBr_4$	4.76	5.34	0.36
$[DMA]_2CoCl_4$	1.77	3.84	1.81

extrapolation of the absorbance from the high slope region obtained from the spectra. It can also be noted that if erroneously the band gap energy is related directly to the absorption peaks, which appear in as-collected UV-Vis spectra, it can lead to overestimate its value with smaller discrepancies. In fact, the values of the band gap energy (E_g) of the samples at room temperature are listed in Table 2. These results are similar to those obtained for other similar hybrid materials[36–40] (Table 3). Then, the calculated E_g values for $[DMA]_2CoCl_4$ crystals are lower than those for $[DMA]_2ZnCl_4$and $[DMA]_2ZnBr_4$. The band gap energy value for $[DMA]_2CoCl_4$ suggests that the material behaves as semiconductor. However, $[DMA]_2ZnCl_4$ and $[DMA]_2ZnBr_4$ compounds can be classified as wide-gap semiconductors. On the other hand, it should be noted that E_g corresponding to $[DMA]_2ZnCl_4$ is lower than that of $[DMA]_2ZnBr_4$.

Therefore, in order to obtain information on the disorder in a material, an Urbach tail analysis was also performed. In this context, Urbach's rule describes the broadening of the absorption edge and the formation of a band tail. Thus, Urbach tail energy (E_u) is introduced to describe the width of the tails due to localized states in the absorption edge.[41] We can access the value of E_u from the following equation:

$$Ln\alpha = Ln\alpha_0 + \frac{h\nu}{E_u}, \quad (2)$$

where α_0 is a constant, E_u represents the Urbach energy (eV) and $h\nu$ is the photon energy (eV).

As seen in Fig. 6(a and b), the tail cannot accurately fit a single slope in the $Ln(\alpha)$ *vs.* photon energy plot. As seen from Table 2, each of the investigated $[DMA]_2MeX_4$ is characterized by its value E_u. These values were similar to the band tails found in the literature (Table 3).[21,37,39,40] It is clear that the energy E_u is higher for the Cl-based compound compared to the Br-based compounds. The large value may be because of the high degree of defect in the cell.[42] Thus, the rate of recombination in perovskite compounds increased as E_u went up because of the rise of the density of the localized states lying deeply between the band gaps.

Table 3 Gap energy and Urbach energy of some hybrid compounds of A_2MX_4 types

Sample	E_g (eV)	E_u (eV)
$[N(CH_3)_4]_2CoCl_4$	4.598 [ref. 36]	—
$[C_8H_{10}NO]_2CoCl_4$	2.98 [ref. 37]	1.27 [ref. 37]
$[N(CH_3)_4]_2ZnCl_4$	5.903 [ref. 38]	0.73 [ref. 21]
$[N(CH_3)_4]_2MnCl_4$	5.419 [ref. 36]	—
$[(C_2H_5NH_3]_2ZnCl_4$	4.04/4.55 [ref. 39]	2.19 [ref. 39]
$[C_8H_{10}NO]_2CdCl_4$	3.17 [ref. 40]	0.622 [ref. 40]

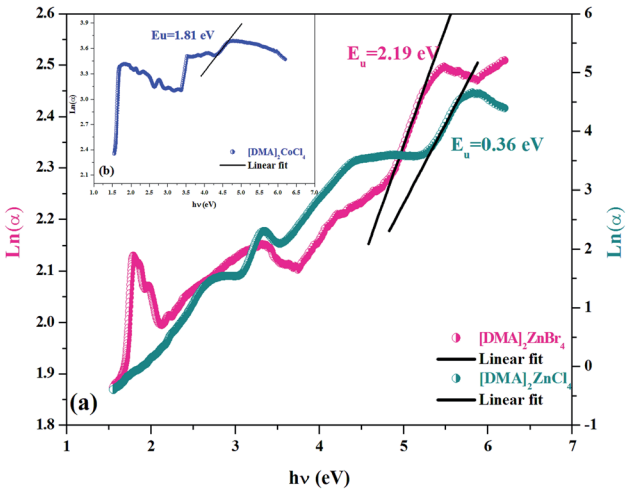

Fig. 6 (a and b) Variation of $Ln(\alpha)$ as a function of ($h\nu$) for $[DMA]_2ZnCl_4$, $[DMA]_2ZnBr_4$ and $[DMA]_2CoCl_4$.

4.4. Optical constants

4.4.1. Extinction coefficient. When optical energy interacts with the matter, it disperses and consequently losses occur, which are described by the extinction coefficient. Then, the absorption coefficient α is related to the extinction coefficient k by:

$$k = \frac{\alpha\lambda}{4\pi}, \quad (3)$$

where k represents the imaginary part of the complex refractive index ($N = n + ik$) and λ is the wavelength of the incident photons, which is responsible for the attenuation of the electromagnetic wave in the medium.

In fact, Fig. 7 shows the plot of the extinction coefficient k as a function of the wavelength λ (nm) for $[DMA]_2ZnCl_4$, $[DMA]_2ZnBr_4$ and $[DMA]_2CoCl_4$. Moreover, the fall and rise in the extinction coefficient are due to the variation of the absorbance. In fact, low values of k indicate the region of transparency of

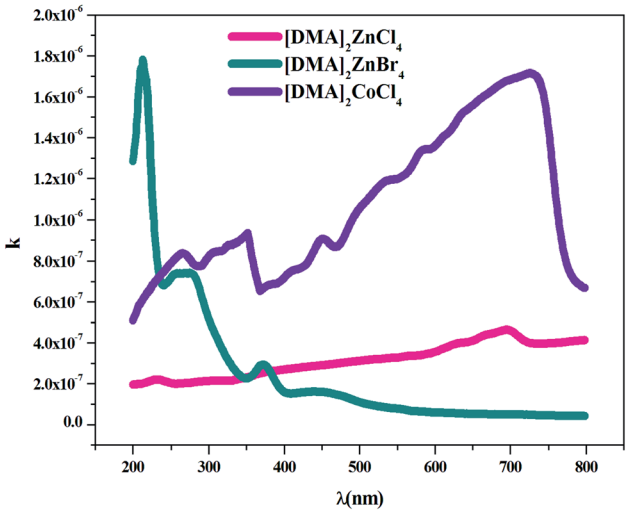

Fig. 7 Variation of the extinction coefficient k as a function of the wavelength λ for $[DMA]_2ZnCl_4$, $[DMA]_2ZnBr_4$ and $[DMA]_2CoCl_4$.

each compound. On the other hand, for the compound dimethylammonium tetrachlorocobaltate, the extinction coefficient k shows several peaks and reaches a maximum in the visible region due to the dark blue color of the crystal. However, the two compounds $[DMA]_2ZnCl_4$ and $[DMA]_2ZnBr_4$ transmit almost most of the incident radiation due to their total transparency in the visible area. In fact, when the crystals exhibit a wide transmission range in the visible domain, they can be used for nonlinear optical applications and antireflection layers of solar thermal devices.[21]

The Br-based compound showed k-values lower than the Cl-based compounds in the visible light spectrum. Therefore, these adequate results justify the use of this material in photovoltaic devices.[43]

4.4.2. Refractive index. The refractive index, which is the result of complex phenomena of interaction between fields and atoms of the matter, can be expressed by:

$$n = \left\{ \left[\frac{4R}{(R-1)^2} - k^2 \right]^{\frac{1}{2}} - \frac{R+1}{R-1} \right\} \quad (4)$$

$$\text{For } k \approx 0 \quad n = \frac{1+\sqrt{R}}{1-\sqrt{R}}, \quad (5)$$

where R is the reflectance of the surface and k is the extinction coefficient. Then, the variation of the (n) index, as a function of the wavelength, can be described by two models; the Cauchy and the Wemple–DiDomenico models.

The Cauchy's formula of the refractive (n) index, as a function of the wavelength λ, is:[44,45]

$$n = n_0 + \frac{A}{\lambda^2} + \frac{B}{\lambda^4}, \quad (6)$$

where (n_0, A et B) correspond to the Cauchy's constants and λ is the wavelength of the incident photons.

Table 4 Calculated values of Cauchy's parameters n_0, A and B

Sample	n_0	A (μm^2)	B (μm^4)
$[DMA]_2ZnCl_4$	4.32	−0.16	1.04×10^{-2}
$[DMA]_2ZnBr_4$	17.55	−3.84	0.266
$[DMA]_2CoCl_4$	2.08	0.08	3.51×10^{-3}

In fact, Cauchy suggests that the refractive index depends primarily on the material and the wavelength. The dependence of the refractive index on the λ (nm) wavelength for $[DMA]_2ZnCl_4$, $[DMA]_2ZnBr_4$ and $[DMA]_2CoCl_4$ is also shown in Fig. 8(a–c), respectively. The increase of the refractive index is due to the increase of the reflectance. The values of n_0, A and B are grouped in Table 4. These estimated values are close to the ones reported by.[41,46] It is clear that n_0 is very large for the compound $[DMA]_2ZnBr_4$ compared to the $[DMA]_2ZnCl_4$ and $[DMA]_2CoCl_4$ compounds. We also notice that for the Cl-based compounds, n is almost constant, that is to say that the variation of n depends very little on λ (A and B are very weak); however, in the compound $[DMA]_2ZnBr_4$, n is very sensitive to the variation of the wavelength (A and B are greater than for the other two compounds).

The concept of the single oscillator suggested by Wemple–DiDomenico describes the evolution of the refractive n index by the following equation:[47–49]

$$n^2 = 1 + \frac{E_0 E_d}{{E_0}^2 - (h\nu)^2}, \quad (7)$$

where E_0 is the single-oscillator energy and E_d the dispersion energy. In fact, E_0 corresponds to the energetic distance between the valence and conduction bands and $h\nu$ is the photon energy (eV). Then, the parameter E_d, which is a measure of the average strength of the inter-band optical transitions, does not significantly depend on the band gap. Moreover, parameters E_0 and E_d for $[DMA]_2ZnCl_4$, $[DMA]_2ZnBr_4$ and $[DMA]_2CoCl_4$ hybrids were calculated from the slope of the linear portion of the plot

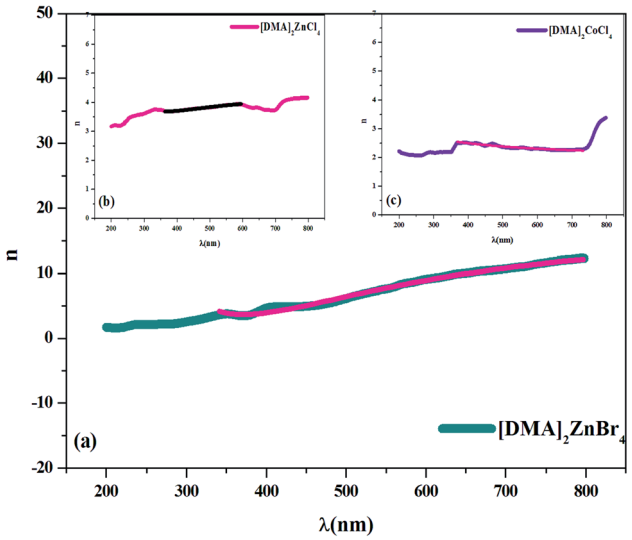

Fig. 8 (a–c) Plot of the refractive index *versus* wavelength λ (nm) for $[DMA]_2ZnBr_4$, $[DMA]_2ZnCl_4$ and $[DMA]_2CoCl_4$, respectively.

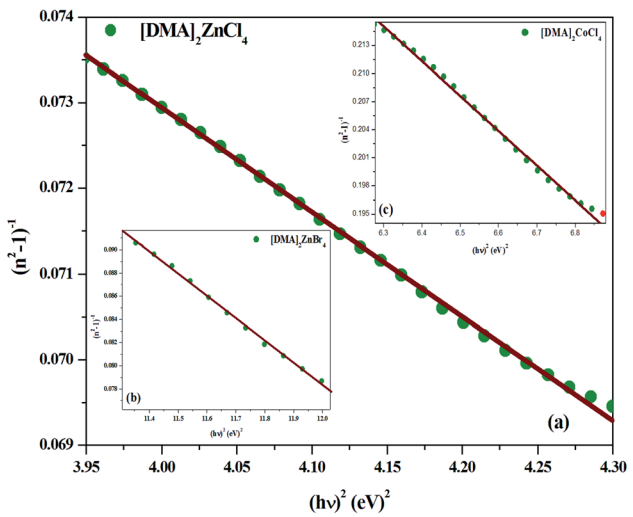

Fig. 9 (a–c) Plots of $(n^2 - 1)^{-1}$ *versus* $(h\nu)^2$ of $[DMA]_2ZnCl_4$, $[DMA]_2ZnBr_4$ and $[DMA]_2CoCl_4$, respectively.

Table 5 Calculated values of E_d, E_0, n_∞, λ_0 and S_0

Sample	E_0 (eV)	E_d (eV)	n_∞	λ_0 (nm)	S_0 (nm^{-2}) × 10^{-5}
$[DMA]_2ZnCl_4$	9.98	8.21	1	316	8.20
$[DMA]_2ZnBr_4$	4	12.98	5.29	356	3.38
$[DMA]_2CoCl_4$	3.47	7741	2.67	309	1.75

$(n^2-1)^{-1}$ *versus* $(h\nu)^2$ as illustrated in Fig. 9(a–c), respectively. Then, the values obtained for the oscillating parameters are gathered in Table 5.

Therefore, the previous equation can be written as follows:

$$n^2 - 1 = \frac{S_0\lambda_0}{1 - \left(\frac{\lambda_0}{\lambda}\right)^2} \quad (8)$$

where λ_0 is the average oscillator wavelength, S_0 corresponds to the oscillator length strength and λ is the wavelength of the incident light. Therefore, in order to determine the values of the long wavelength refractive (n_∞), index average oscillator wavelength λ_0 and the average oscillator strength (S_0) for the samples, we can use the following relationship:

$$\frac{{n_\infty}^2 - 1}{n^2 - 1} = 1 - \left(\frac{\lambda_0}{\lambda}\right)^2 \quad (9)$$

and

$${n_\infty}^2 = 1 + S_0{\lambda_0}^2 \quad (10)$$

The plot of $(n^2-1)^{-1}$, as a function of $(1/\lambda^2)$, gives a linear part (Fig. 10(a–c)) for $[DMA]_2ZnCl_4$, $[DMA]_2ZnBr_4$, $[DMA]_2CoCl_4$, successively. In fact, Table 5 shows the values of n_∞, λ_0 and S_0.

On the other hand, for the development of optical applications of the optical material under study, determining the moments of the spectrum is very necessary. Therefore, the M_{-1} and M_{-3} moments can be determined by the following equations:

Table 6 Calculated values of M_{-1} and M_{-3}

Sample	M_{-1} ((eV)$^{-2}$)	M_{-3} ((eV)$^{-2}$)
$[DMA]_2ZnCl_4$	0.82	0.00825
$[DMA]_2ZnBr_4$	3.23	0.20096
$[DMA]_2CoCl_4$	2.22	0.18373

$$E_0{}^2 = \frac{M_{-1}}{M_{-3}} \quad (11)$$

And,

$$E_d{}^2 = \frac{{M_{-1}}^3}{M_{-3}} \quad (12)$$

The M_{-1} and M_{-3} values of for $[DMA]_2ZnCl_4$, $[DMA]_2ZnBr_4$ and $[DMA]_2CoCl_4$ compound are summarized in Table 6. Then, the obtained M^{-1} and M^{-3} are slightly elevated for the compound $[DMA]_2ZnBr_4$. These moments determine the average bond strength. Eqn (11) and (12) indicates a single-oscillator approximation to the dielectric response of these materials. The optical moments are related to the macroscopic quantities, like the effective dielectric constant, the effective number of valence electrons in the investigated material.[50]

4.4.3. Dielectric constant. Several theoretical models have been developed to study the dielectric constants for material applications in optoelectronic devices, which characterize the optical properties of a solid material. In fact, the real part (ε_r) of the dielectric constant shows how much it will slow down the speed of light in the material, whereas the imaginary part (ε_i) represents the absorption of the associated radiation by free carriers. The complex dielectric constant ε is related to the refractive index (n) and the extinction coefficient (k) as:[49]

$$\varepsilon = \varepsilon_r + i\varepsilon_i, \quad (13)$$

$$\varepsilon_r = n^2 - k^2, \quad (14)$$

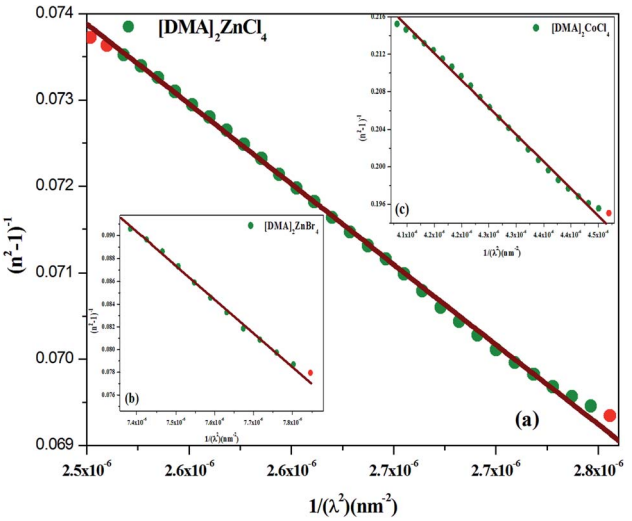

Fig. 10 (a–c) Plots of $(n^2\text{-}1)^{-1}$ *versus* $1/\lambda^2$ of $[DMA]_2ZnCl_4$, $[DMA]_2ZnBr_4$ and $[DMA]_2CoCl_4$, respectively.

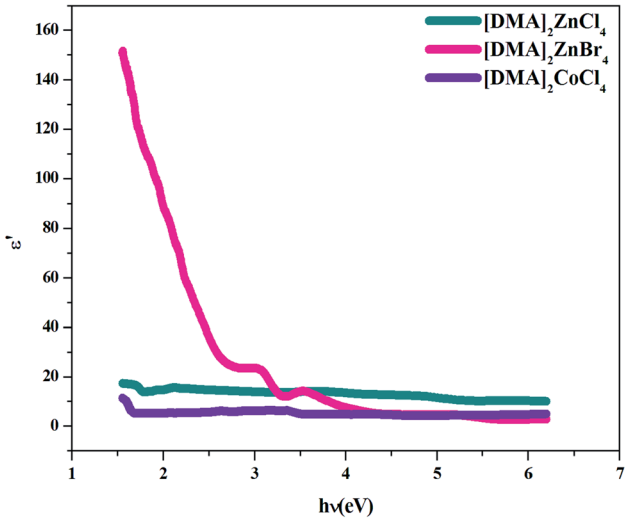

Fig. 11 Real part ε' of the dielectric permittivity *versus* $(h\nu)$ for $[DMA]_2ZnCl_4$, $[DMA]_2ZnBr_4$ and $[DMA]_2CoCl_4$.

$$\varepsilon_i = 2nk, \quad (15)$$

Additionally, studies of the real and imaginary parts of the dielectric constant give us the information about the loss factor, which is the ratio of the imaginary part to the real part of the dielectric constant. Then, the variation of the real and imaginary part of the dielectric constant with the incident photon energy for the $[DMA]_2ZnCl_4$, $[DMA]_2ZnBr_4$, $[DMA]_2CoCl_4$ sample were determined and shown in Fig. 11 and 12.

On the other hand, the extinction coefficient has a negligible contribution (in the order of 10^{-6}) whereas the refractive index has a comparatively very high value. An increase of the real part was observed with the increase of the photon energy. Consequently, the real part of the dielectric constant depends only on the refractive index by eqn (7). For the $[DMA]_2ZnBr_4$ compound, the calculated real dielectric constant values are very high (10–155) at the particular interest of the visible region. The imaginary part of the dielectric constant depends on the extinction coefficient by eqn (8). As can be seen from Fig. 12, different shapes of the curves for the imaginary part of the dielectric constant have been observed. Therefore, the imaginary part confirms the free carrier contribution to the absorption. We notice that the imaginary part of the complex permittivity (in the order of 10^{-6}) is very low compared to the real part.

4.4.4. Optical conductivity. Optical conductivity is a significant tool for studying the electronic states in materials. In general, if an external electric field is applied, a redistribution of charges occurs and currents are induced. Fig. 13 shows the variation of optical conductivity with the incident photon energy. Optical conductivity was determined using the relation:[51,52]

$$\sigma = \alpha nc/4\pi, \quad (16)$$

where c is the velocity of light and α is the absorption coefficient.

The increased optical conductivity is due to the high absorbance of the sample in that region. The optical conductance and band gap indicated that $[DMA]_2ZnCl_4$ and $[DMA]_2ZnBr_4$ have high transmittance compared to $[DMA]_2CoCl_4$ within the visible range.

The maximum value of conductivity for the compound $[DMA]_2ZnBr_4$ (4×10^{10} s^{-1}) is greater than that of the two compounds $[DMA]_2ZnCl_4$ (5.5×10^9 s^{-1}) and $[DMA]_2CoCl_4$ (1.5×10^{10} s^{-1}). Besides that, these high values of the optical conductivity of $[DMA]_2ZnBr_4$ pointed out to the superiority of the material for such photovoltaic applications.[53]

4.5. Dielectric relaxation

The dielectric properties are correlated with the electro-optic properties of the prepared crystals. Therefore, the dielectric relaxation studies are important to provide the conduction processes ($T_g\delta = \varepsilon''/\varepsilon' \gg 10$), since it enables to determine the origin of the dielectric losses.[54] Then, in order to obtain more information about $[DMA]_2ZnBr_4$, $[DMA]_2CoCl_4$ and $[DMA]_2ZnCl_4$ dynamic compounds, we measured the impedance spectra of the sample at room temperature from which we derived the frequency-dependent dielectric constant (ε') and the loss tangent ($T_g(\delta)$) in the frequency range of 10^{-1} to 10^7 Hz.

The frequency dependence of the dielectric constant is depicted in Fig. 14. It is clearly that ε' shows dispersions at low frequencies and gets almost saturated at higher frequencies. Such dispersions in both components of the complex dielectric constant are referred to as low frequency dielectric dispersion (LEDD) and are associated with the space charge accumulation effect and/or conducting ion motion. The observed sharp decrease of ε' as frequency increases is mainly due to the space charges contributing to the high permittivity in the materials. The magnitude of the dielectric constant depends on the degree of polarization and the charge displacement in crystal. It can be observed that ε' approaches a limiting constant value (ε'_∞), at high frequencies, which can be attributed to the absence of space charge polarization near the grain boundary interface. Moreover, with the increase of frequency, ε' becomes almost parallel. In fact, the most striking feature is that there are no

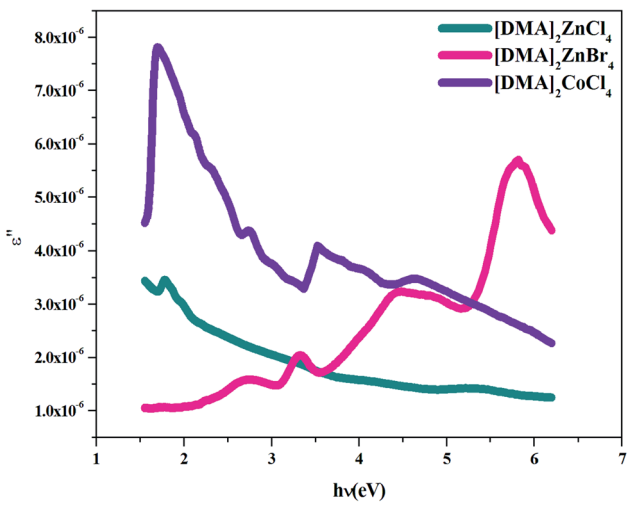

Fig. 12 Imaginary part ε' of the dielectric permittivity *versus* ($h\nu$) for $[DMA]_2ZnCl_4$, $[DMA]_2ZnBr_4$ and $[DMA]_2CoCl_4$.

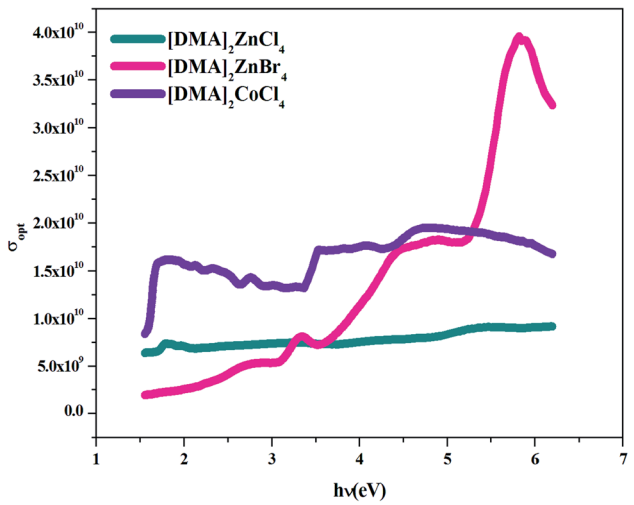

Fig. 13 σ_{opt} *versus* ($h\nu$) for $[DMA]_2ZnCl_4$, $[DMA]_2ZnBr_4$and $[DMA]_2CoCl_4$.

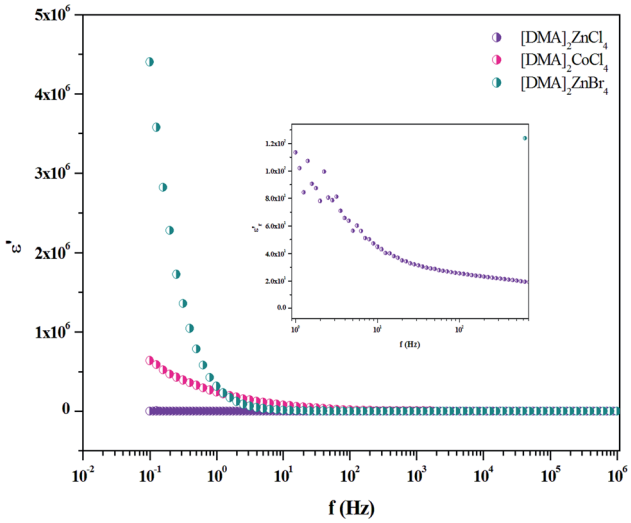

Fig. 14 Variation of ε' *versus* frequency for $[DMA]_2ZnCl_4$, $[DMA]_2ZnBr_4$ and $[DMA]_2CoCl_4$ matrix at room temperature.

relaxation peaks observed in the frequency range employed in this study. The dielectric constant decreases from a low frequency value of about $\approx$155 for $[DMA]_2ZnCl_4$, $\approx 2 \times 10^5$ for $[DMA]_2CoCl_4$ and $\approx 4 \times 10^6$ for $[DMA]_2ZnBr_4$ to the high frequency value in the order of ten. Then, the high dielectric constant of $[DMA]_2ZnBr_4$, implies that this compound could be a candidate in energetic devices. Indeed, materials of a large dielectric constant can be used as a dielectric gate or an active channel in FET devices.[55]

The analysis of Fig. 15 describing $T_g(\delta)$ revealed one relaxation peak for each hybrid. This peak is noticed at the frequencies of 10^2, $7 \times 10^3$and 10^4 Hz for $[DMA]_2ZnBr_4$, $[DMA]_2CoCl_4$ and $[DMA]_2ZnCl_4$, respectively. Considering the low frequency and the broad peak feature, this relaxation process could be a Maxwell–Wagner type interfacial polarization relaxation, possibly attributed to grain boundary effects or blocking at the

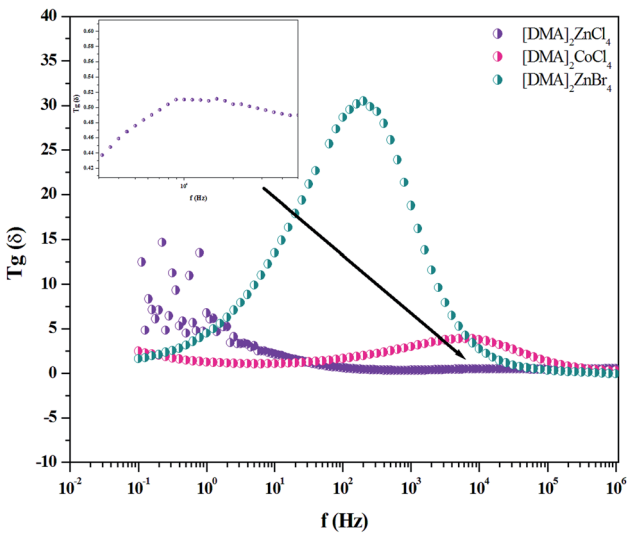

Fig. 15 Variation of $T_g(\delta)$ *versus* frequency for $[DMA]_2ZnCl_4$, $[DMA]_2ZnBr_4$and $[DMA]_2CoCl_4$ matrix at room temperature.

contacts. From the graph, it is clear that the for $[DMA]_2ZnBr_4$, $[DMA]_2CoCl_4$ and $[DMA]_2ZnCl_4$, the crystals exhibit very low dielectric loss at high frequencies, which can be a potential candidate for nonlinear optics NLO applications.[56]

5. Conclusions

In the present study, the powder XRD study of $[DMA]_2ZnCl_4$, $[DMA]_2ZnBr_4$ and $[DMA]_2CoCl_4$ crystals confirmed the lattice parameter values. The optical properties, which are of scientific importance, were investigated by optical spectroscopy (UV-visible). The obtained results show a significant difference in the absorption spectra among $[DMA]_2ZnCl_4$, $[DMA]_2ZnBr_4$ and $[DMA]_2CoCl_4$ sample. The Tauc model was used to determine the optical band gap energy values. In fact, the values of (E_{gi}, E_{gd}) are (1.91, 4.29) eV for $[DMA]_2ZnCl_4$, (4.76, 5.34) eV for $[DMA]_2ZnBr_4$ and (1.77, 3.84) eV for $[DMA]_2CoCl_4$ are in conformity with the reported values for other similar hybrid materials, specially $[TMA]_2MeCl_4$ (Me = Co, Zn, …) compounds. It can be observed that the band gap of all the samples lie in the range of semiconductors. Then, the observed variation in optical parameters, such as the refractive index (n), the extinction coefficient (k), the optical conductivity (σ_{opt}), and the dielectric constants (ε*) have been evaluated and show sufficient agreement with the values reported for some A_2BX_4 family single crystals. The refractive index values have been fitted to the single oscillator Wemple–DiDomenico (WDD) model. The single oscillator energy (E_0), the dispersion energy (E_d), the static refractive index n_0, the moments of the optical dispersion spectra M_{-1} and M_{-3}, the static refractive index n_∞ and the oscillator strength S_0 were estimated at room temperature, which showed sufficient agreement with the values reported for the A_2BX_4 family. On the other hand, the electrical properties of the high dielectric constant at low frequencies, suggest that $[DMA]_2ZnBr_4$ could be used in the energy devices. In fact, the low dielectric constant and the low dielectric loss at high frequencies, suggest that the $[DMA]_2ZnCl_4$, $[DMA]_2ZnBr_4$ and $[DMA]_2CoCl_4$ crystalline compounds could be used in nonlinear optoelectronic devices.

Conflicts of interest

There are no conflicts to declare.

References

1 M. Suchańska, S. Kałuża and S. Leśniewski, *Opto-Electron. Rev.*, 2001, **9**, 353–355.
2 C. L. Folca, J. M. Pérez-Mato and M. J. Tello, *Solid State Commun.*, 1990, **74**, 717–720.
3 I. M. Shmyt'ko and B. S. Bagautdinov, *Crystallogr Rep*, 1998, **43**, 631–639. Translated from, *Kristallografiya*, **43**, 1998, 680–687.
4 A. Yu Oleshchuk, G. A. Kiosse, Z. A. Bobrova, L. A. Shuvalov and T. I. Malinovskii, *Sov. Phys. Crystallogr.*, 1989, **34**, 690.
5 A. R. Lim and K.-Y. Lim, *Solid State Sci.*, 2014, **31**, 70.

6 O. G. Vlokh, V. B. Kapustyanyk, I. I. Polovinko, S. A. Sveleba, V. M. Varikash and Z. A. Bobrova, *Zh. Prikl. Spektrosk.*, 1990, **52**, 785.
7 A. U. Sheleg, T. I. Dekola and N. P. Tekhanovich, *Phys. Solid State*, 2003, **45**, 946.
8 V. E. Vasil'ev, V. M. Rudyak, Z. A. Bobrova and V. M. Varikash, *Sov. Phys. Solid State*, 1987, **29**, 882.
9 N. Mahfoudh, K. Karoui, K. Khirouni and A. Ben Rhaiem, *Phys. B*, 2019, **455**, 126–136.
10 A. H. Mahmoudkhani and V. Langer, *Acta Crystallogr., Sect. B: Struct. Sci.*, 1999, **55**, 752.
11 N. Mahfoudh, K. Karoui, M. Gargouri and A. Ben Rhaiem, *Appl. Organomet. Chem.*, 2020, **34**, 5404.
12 N. Mahfoudh, K. Karoui, F. Jomni and A. Ben Rhaiem, *Appl. Organomet. Chem.*, 2020, **34**, 5656.
13 V. B. Kapustianik, S. A. Sveleba, R. Tchukvinskyi, Y. u. Korchak, V. Mokryi, I. I. Polovinko and Z. Trybula, *Phys. Stat. Sol.*, 1995, **151**, 481–488.
14 C.-L. Ho, H. Li and W.-Y. Wong, *J. Organomet. Chem.*, 2014, **751**, 261–285.
15 C. Sanchez, B. Lebeau, F. Chaput and J. P. Boillot, *Adv. Mater.*, 2003, **15**, 1969.
16 C. Sanchez, B. Juliàn, P. Belleville and M. Popall, *J. Mater. Chem.*, 2005, **15**, 3559.
17 C. Sanchez, G. J. Soler-Illia, F. Ribot, T. Lalot, C. R. Mayer and V. Cabuil, *Chem. Mater.*, 2001, **13**, 3061.
18 Y. Zhang and B. Champagne, *J. Phys. Chem. C*, 2013, **117**, 1833–1848.
19 M. R. S. A. Janjua, S. Jamil, T. Ahmad, Z. Yang, A. Mahmood and S. Pan, *Comput. Theor. Chem.*, 2014, **1033**, 6–13.
20 D. Osella, L. Milone, C. Nervi and M. Ravera, Electronic interactions in organometallic dimers. An electrochemical approach, *J. Organomet. Chem.*, 1995, **488**, 1–7.
21 A. Abu El-Fadl and A. M. Nashaat, *Open Mater. Sci. J.*, 2015, **9**, 162–172.
22 *Celref program*, http://www.ccp14.ac.uk/tutorial/lmgp/celref.htm.
23 C. Ben Mohamed, K. Karoui, M. Tabellout and A. Ben Rhaiem, *J. Alloy. Compd.*, 2016, **688**, 407–415.
24 S. Devashankar, L. Mariappan, P. Sureshkumar and M. Rathnakumari, *J. Cryst. Growth*, 2009, **311**, 4207–4212.
25 S. Kalyanaraman, P. M. Shajinshinu and S. Vijayalakshmi, *Phys. B*, 2016, **482**, 38–42.
26 A. B. P. Lever, *Inorganic Electronic Spectroscopy*, Mir, Moscow, 1987.
27 A. El-Korashy and M. G. Brik, *Solid State Commun.*, 2005, **135**, 298–303.
28 H. W. Smith and W. J. Stratton, *Inorg. Chem.*, 1977, **16**, 1640.
29 F. A. Yassin, F. Y. El Kady, H. S. Ahmed, L. K. Mohamed, S. A. Shaban and A. K. Elfadaly, *Egypt. J. Petrol*, 2015, **24**, 103.
30 V. B. Kapustianik, *Phys. Stat. Sol*, 1998, **207**, 509.
31 A. Abkari, I. Chaabane and K. Guidara, *J. Phys. E*, 2017, **86**, 210.
32 S. Chaouachi, S. Elleuch, B. Hamdi and R. Zouari, *J. Mol. Struct.*, 2016, **1125**, 149.
33 Science News Online (6/6/98): Melanoma Madness The scientific flap over sunscreens and skin cancer – Chemical studies (accessed 10/1/2009, 2009).
34 J. Tauc, *Amorphous and Liquid Semiconductor*, Plenum Press, New York, (1979).
35 H. Ammar, A. A. M. Farag and M. S. Abo-Ghazala, *J. Alloy. Compd*, 2017, **694**, 752–760.
36 A. El-Korashy, H. El-Zahed and M. Radwan, *Phys. B*, 2003, **334**, 75–81.
37 A. Abkari, I. Chaabane and K. Guidara, *Phys. E*, 2017, **86**, 210–217.
38 A. Abu El-Fadl, M. Almokhtar and A. M. Nashaat, *Open J. Appl. Sci.*, 2015, **5**, 169–181.
39 C. Ben Mohamed, K. Karoui and A. Ben Rhaiem, *Phase Transitions*, 2018, **91**, 1162–1178.
40 A. Jellibi, I. Chaabane and K. Guidara, *J. Phys. E*, 2016, **79**, 167–172.
41 M. V. Kruik, Urbach rule, *Phys. Status Solidi A*, 1971, **8**, 9–45.
42 S. A. Moyez and S. Roy, *J. Nanopart. Res.*, 2017, **20**, 5.
43 S. B. Khan, S. Irfan, Z. Zhuanghao and S. L. Lee, *Materials*, 2019, **12**, 1483.
44 H. G. Tompkins and W. A. McGahan, *Spectroscopic Ellipsometry and Reflectometry*, John Wiley and Sons Inc., New York, 1999.
45 B. Ouni, A. Boukhachem, S. Dabbous, A. Amlouk, K. Boubaker and M. Amlouk, *Mater. Sci. Semicond. Process.*, 2010, **13**, 281–287.
46 H. Kchaou, K. Karoui, K. Khirouni and A. Ben Rhaiem, *J. Alloys Compd.*, 2017, 728–936.
47 S. H. Wemple and M. Didomenico, *J. Appl. Phys.*, 1969, **40**, 720.
48 S. H. Wemple and M. Didomenico, *Phys. Rev. B: Condens. Matter Mater. Phys.*, 1971, **3**, 1338.
49 M. A. Omar, *Elementary Solid State Physics*, Addison-Wesley Publishing Company, New York, 1993.
50 M. Okutan, S. Eren San, O. Koysal and F. Yakuphanoglu, *Phys. B*, 2005, **362**, 180.
51 S. Asha, Y. Sangappa and S. Ganesh, *J. Spectrosc.*, 2015, **7**, 1–7.
52 N. A. Bakr, A. M. Funde, V. S. Waman, *et al.*, *J. Phys.*, 2011, **76**(3), 519–531.
53 M. Gratzel, *Nat. Mater.*, 2014, **13**(9), 838–842.
54 A. C. Dhieb, A. Valkonen, M. Rzaigui and W. Smirani, *J. Mol. Struct.*, 2015, **1102**, 50–60.
55 E. J. Juarez-Perez, R. S. Sanchez, L. Badia, G. Garcia-Belmonte, Y. S. Kang, I. Mora-Sero and J. Bisquert, *J. Phys. Chem. Lett.*, 2014, **5**, 2390.
56 D. Balasubramanian, P. Murugakoothan and R. Jayavel, *J. Cryst. Growth*, 2010, **312**, 1855–1859.